Letters

An Optimized Modulation of Three-Phase Buck Rectifier With CM Filter for DC-Link Current Ripple Suppression

Fei Xie, Jianping Xu, *Member, IEEE*, Xiaoqiang Wang, and Kai Liu

***Abstract*—In high-frequency and high-power-density application, common-mode (CM) filter is often incorporated into a three-phase buck rectifier (3ph-BR) to mitigate CM noise. The CM filter in the 3ph-BR has a serious effect on its dc-link current. Accordingly, for the 3ph-BR with CM filter, conventional modulations are ineffective to suppress the dc-link current ripple. In order to solve this issue, an improved modulation is proposed in this letter. By optimizing the vector pattern, the dc-link inductors of the 3ph-BR complete two charging and discharging cycles in one switching period. The dc-link current ripples are thus suppressed. A 1-kW prototype is built and experimental results are provided. Compared to the conventional modulation, the proposed modulation reduces dc-link current ripple by approximately 50%.**

***Index Terms*—DC-link current ripple, high density, three-phase buck rectifier (3ph-BR).**

I. Introduction

DUE to its advantage of low total harmonic distortion (THD) of input currents and high reliability [1], [2], the three-phase buck rectifier (3ph-BR) has been widely used in many applications, e.g., electrical vehicle charging [3] and more electric aircraft [4]. The dc-link current ripple is one of the key issues of 3ph-BR, which not only affects the inductor loss but also affects the THD of the input currents [5]. By reducing the dc-link current ripple, smaller inductance can be used. The reduction of inductor size contributes to improved power density and a more compact converter design.

The dc-link current ripple is closely related to the modulation scheme [6]. The optimization of the modulation scheme provides an effective way to reduce the dc-link current ripple without additional hardware costs. Thus, various modulation schemes have been reported to suppress the dc-link current ripple of 3ph-BR [7], [8], [9].

Received 11 August 2025; revised 26 September 2025 and 11 November 2025; accepted 26 November 2025. Date of publication 28 November 2025; date of current version 19 January 2026. This work was supported by the National Natural Science Foundation of China under Grant 52477198 and Grant 52307019. *(Corresponding authors: Jianping Xu; Xiaoqiang Wang.)*

The authors are with the School of Electrical Engineering, Southwest Jiaotong University, Chengdu 611756, China, and also with the Key Laboratory of Magnetic Suspension Technology and Maglev Vehicle, Ministry of Education, Chengdu 611756, China (e-mail: pcc_xf@my.swjtu.edu.cn; jpxu@swjtu.edu.cn; xqwang06@swjtu.edu.cn; lk0513@my.swjtu.edu.cn).

Color versions of one or more figures in this article are available at https://doi.org/10.1109/TPEL.2025.3638799.

Digital Object Identifier 10.1109/TPEL.2025.3638799

In [7], an optimal space vector modulation is proposed to reduce the dc-link current ripple of 3ph-BR. By eliminating the zero vector and using three active vectors, the proposed modulation reduces the dc-link current ripple effectively. However, it has a minimum modulation index constraint of 0.577, thereby limiting its application. To solve this issue, a direct phase-disposition carrier-based modulation (DPD-CBM) scheme is proposed in [8]. By adaptively selecting vector patterns according to the modulation index, it can mitigate the dc-link current ripple within the full modulation index range. However, due to the employment of the non-nearest active vectors, the switching harmonic is higher than that of the conventional modulation.

Based on the virtual space vector strategy, a dc-link current ripple suppression strategy of the three-phase current source converter is proposed [9]. The dc-link current ripple under virtual active vector is analyzed. By avoiding the large variation of the bridge output voltage, the proposed modulation reduces the dc-link current ripple effectively.

The aforementioned modulation schemes are designed for conventional 3ph-BR [7], [8], [9]. In high-frequency and high-power-density application, the parasitic capacitances distributed between the dc-link output and the system ground will cause serious common-mode (CM) noise, which leads to distorted input currents [10]. Thus, the CM filter is often added in the 3ph-BR to mitigate the CM noise [10], [11], [12]. The dc-link current ripple characteristic of the 3ph-BR with CM filter is different from that of the conventional 3ph-BR without CM filter. Thus, conventional dc-link current ripple suppression methods are ineffective for the 3ph-BR with CM filter.

To suppress the dc-link current ripple of the 3ph-BR with CM filter, an optimized modulation is proposed in this letter. The dc-link current ripple of the 3ph-BR with CM filter is analyzed. Based on this, by optimizing the vector pattern, the dc-link inductors complete two charging and discharging cycles in one switching period, i.e., the current ripples are suppressed. The effectiveness of the proposed modulation is demonstrated by experimental results.

II. Analysis of the DC-Link Current Ripple of the 3ph-BR With CM Filter

Fig. 1 shows the circuit topology of the 3ph-BR with a CM filter. It consists of an input filter, switch unit, CM filter, and

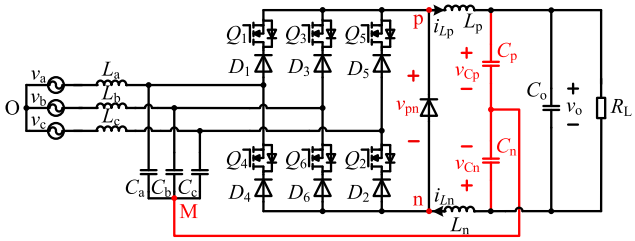

Fig. 1. Circuit topology of the 3ph-BR with CM filter.

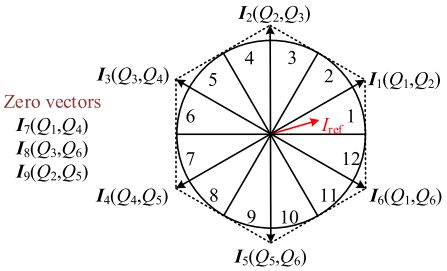

Fig. 2. Current space vector diagram.

TABLE I
RELATIONSHIP BETWEEN CURRENT VECTORS AND THE BRIDGE OUTPUT VOLTAGE

Vector	I_1	I_2	I_3	I_4	I_5	I_6	I_7	I_8	I_9
v_{pM}	v_a	v_b	v_b	v_c	v_c	v_a	v_a	v_b	v_c
v_{nM}	v_c	v_c	v_a	v_a	v_b	v_b	v_a	v_b	v_c
v_{pn}	v_{ac}	v_{bc}	v_{ba}	v_{ca}	v_{cb}	v_{ab}	0	0	0

output filter. The CM filter consists of capacitors C_p and C_n, with their common point M connected to the neutral point of the input filter capacitors. As demonstrated in [10], the CM filter effectively blocks CM current flowing to the input side.

The diagram of the current space vector is shown in Fig. 2. There are six active vectors $\boldsymbol{I}_1$–$\boldsymbol{I}_6$ and three zero vectors $\boldsymbol{I}_7$–$\boldsymbol{I}_9$. The space is divided into 12 sectors, with different sectors employing different vectors to synthesize the reference vector. For simplicity, it is assumed that the voltages on the input filter capacitors are equal to the input phase voltages. The relationship between current vectors and voltages v_{pM}, v_{nM}, and v_{pn} is summarized, as shown in Table I.

For the 3ph-BR without the CM filter, the currents and the voltages of the inductors L_p and L_n are equal. Thus, the dc-link current ripple $\triangle i_L$ can be calculated as

$$\Delta i_L = \frac{v_{pn} - v_o}{L_p + L_n}\Delta t \tag{1}$$

where $\triangle t$ is the charging time or the discharging time of the inductor current. It can be found from (1) that $\triangle i_L$ of the conventional 3ph-BR without CM filter is related to the bridge output voltage v_{pn}. Thus, by adjusting the vector sequence to optimize the variation of v_{pn}, $\triangle i_L$ is reduced [7], [8], [9].

Different from the conventional 3ph-BR without the CM filter, the currents and voltages of the inductors L_p and L_n in the 3ph-BR with the CM filter are not equal. The dc-link current ripples

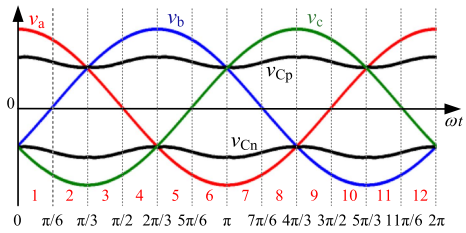

Fig. 3. Input voltages and voltages v_{Cp}, v_{Cn}.

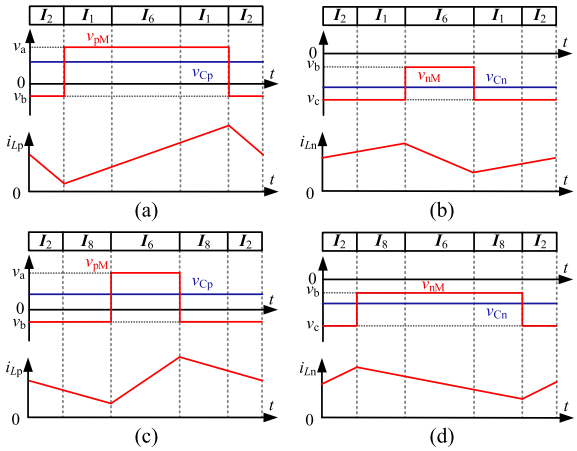

Fig. 4. Waveforms of $v_{\rm pM}$, $v_{\rm nM}$, and i_{Lp}, i_{Ln} with the conventional DPD-CBM in sector 1. (a) v_{pM} and i_{Lp} when m>0.577. (b) v_{nM} and i_{Ln} when m>0.577. (c) v_{pM} and i_{Lp} when m<0.577. (d) v_{nM} and i_{Ln} when m<0.577.

$\triangle i_{Lp}$ and $\triangle i_{Ln}$ can be calculated as

$$\begin{cases} \Delta i_{Lp} = \frac{v_{pM} - v_{Cp}}{L_p}\Delta t \\ \Delta i_{Ln} = \frac{-v_{nM} + v_{Cn}}{L_n}\Delta t \end{cases} \tag{2}$$

where v_{Cp} and v_{Cn} are the voltages on the capacitors C_p and C_n, respectively. It can be seen from (2) that $\triangle i_{Lp}$ and $\triangle i_{Ln}$ are related to v_{Cp}, v_{Cn}, v_{pM}, and v_{nM}. The averages of v_{Cp} and v_{Cn} are independent of modulation, which are derived in [10], and thus will not be repeated in this letter. According to the calculation result in [10], v_{Cp}, v_{Cn} are plotted in Fig. 3.

The voltages v_{pM} and v_{nM} are determined by current vectors, i.e., they can be optimized by modulation, thereby reducing $\triangle i_{Lp}$ and $\triangle i_{Ln}$. However, conventional modulations are designed to optimize the variation of v_{pn} [7], [8], [9]. Thus, they cannot suppress the dc-link current ripple of the 3ph-BR with the CM filter.

Taking the DPD-CBM [8] and the switching loss optimized (SLO) modulation [10] as examples to analyze the current ripple. For the DPD-CBM, the zero vector is employed for low modulation index m, and is eliminated for high modulation index m. Thus, the DPD-CBM has two vector patterns according to m. By using the vector pattern without zero vector, the minimum m is $\sqrt{3}/3 \approx 0.577$. Thus, the current ripple is analyzed in two cases, i.e., m>0.577 or m<0.577.

Fig. 4 shows v_{pM}, v_{nM}, i_{Lp}, and i_{Ln} in sector 1 by using DPD-CBM, where the vector sequences are $\boldsymbol{I}_2$-$\boldsymbol{I}_1$-$\boldsymbol{I}_6$-$\boldsymbol{I}_1$-$\boldsymbol{I}_2$ and $\boldsymbol{I}_2$-$\boldsymbol{I}_8$-$\boldsymbol{I}_6$-$\boldsymbol{I}_8$-$\boldsymbol{I}_2$ when m>0.577 and m<0.577, respectively. For

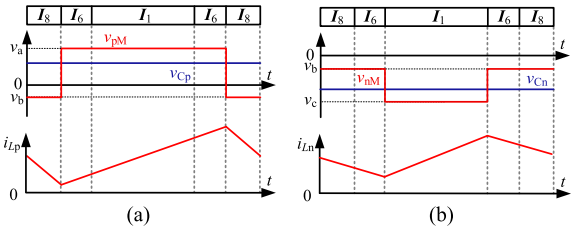

Fig. 5. Waveforms of $v_{\rm pM}$, $v_{\rm nM}$ and i_{Lp}, i_{Ln} with the conventional SLO modulation in sector 1. (a) v_{pM} and i_{Lp}. (b) v_{nM} and i_{Ln}.

TABLE II
VECTOR PATTERNS OF THE PROPOSED MODULATION IN 12 SECTORS

Sector	Vector pattern	Sector	Vector pattern
1	I_8, I_1, I_6, I_8, I_1	2	I_8, I_1, I_8, I_1, I_2
3	I_7, I_2, I_1, I_7, I_2	4	I_7, I_2, I_7, I_2, I_3
5	I_9, I_3, I_2, I_9, I_3	6	I_9, I_3, I_9, I_3, I_4
7	I_8, I_4, I_3, I_8, I_4	8	I_8, I_4, I_8, I_4, I_5
9	I_7, I_5, I_4, I_7, I_5	10	I_7, I_5, I_7, I_5, I_6
11	I_9, I_6, I_5, I_9, I_6	12	I_9, I_6, I_9, I_6, I_1

L_p, i_{Lp} increases under $\boldsymbol{I}_1$ or $\boldsymbol{I}_6$ while decreases under $\boldsymbol{I}_2$ or $\boldsymbol{I}_8$. For L_n, i_{Ln} increases under $\boldsymbol{I}_1$ or $\boldsymbol{I}_2$ while decreases under $\boldsymbol{I}_6$ or $\boldsymbol{I}_8$. Thus, whether m>0.577 or m<0.577, both L_p and L_n have only one charging/discharging cycle, i.e., the current ripples are not reduced.

Fig. 5 shows v_{pM}, v_{nM}, i_{Lp}, and i_{Ln} in sector 1 by using SLO, where the vector sequence is $\boldsymbol{I}_8$-$\boldsymbol{I}_6$-$\boldsymbol{I}_1$-$\boldsymbol{I}_6$-$\boldsymbol{I}_8$. Though the vector sequence of SLO is different from that of DPD-CBM, both L_p and L_n still have one charging/discharging cycle; the current ripples are thus not suppressed either.

III. PROPOSED DC-LINK CURRENT RIPPLE SUPPRESSION MODULATION FOR 3PH-BR WITH CM FILTER

A. Proposed DC-Link Current Ripple Suppression Method

In order to suppress the dc-link current ripple of the 3ph-BR with CM filter, an optimized modulation is proposed in this section. Table II shows the vector sequences of the proposed modulation in 12 sectors. It can be seen from Table II that the non-nearest vector is not employed, which can suppress the harmonics of input currents [8]. Compared to DPD-CBM, which uses non-nearest vectors, the proposed modulation has a lower THD of input currents.

In the proposed modulation, the dwell times of one active vector and zero vector are divided into two parts. Taking sector 1 as an example, the dwell times of the two parts of vectors $\boldsymbol{I}_1, \boldsymbol{I}_8$ are denoted as $T_{1\text{-}1}$, $T_{1\text{-}2}$ and $T_{8\text{-}1}$, $T_{8\text{-}2}$, respectively, as shown in Fig. 6. Therefore, it has

$$\begin{cases} T_6 = -mT_s v_b / V_m \\ T_1 = T_{1-1} + T_{1-2} = -mT_s v_c / V_m \\ T_8 = T_{8-1} + T_{8-2} = T_s - mT_s v_a / V_m \end{cases} \tag{3}$$

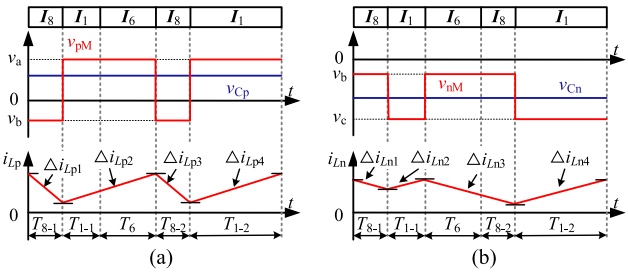

Fig. 6. Waveforms of $v_{\rm pM}$, $v_{\rm nM}$ and i_{Lp}, i_{Ln} with the proposed modulation in sector 1. (a) v_{pM} and i_{Lp}. (b) v_{nM} and i_{Ln}.

where T_6, T_1, and T_8 are dwell times of vectors $\boldsymbol{I}_6$, $\boldsymbol{I}_1$, and $\boldsymbol{I}_8$, respectively, T_s is the time of one switching period, and V_m is the maximum of the input phase voltage.

In sector 1, the peak-peak value of $\triangle i_{Lp}$ is larger than that of $\triangle i_{Ln}$, thus, the reduction of $\triangle i_{Lp}$ is in priority, which can be achieved by dividing the charging/discharging time of L_p into two equal time periods. The discharging time of L_p is T_8, thus, it has $T_{8\text{-}1} = T_{8\text{-}2} = 0.5T_8$, and the charging time of L_p is $T_{1\text{-}1}$+$T_{1\text{-}2}$+T_6, it thus has

$$\begin{cases} T_{1-1} = (T_1 - T_6)/2 \\ T_{1-2} = (T_1 + T_6)/2 \end{cases}. \tag{4}$$

It can be known from (4) that $T_{1\text{-}2} = T_{1\text{-}1}$+$T_6$, i.e., the charging time of L_p is divided into two equal time periods. Therefore, $\triangle i_{Lp}$ can be optimized, as shown in Fig. 6(a). It can be seen that inductor L_p has two charging/discharging cycles. In addition, the proposed method can optimize $\triangle i_{Ln}$, as inductor L_n also has two charging/discharging cycles, as shown in Fig. 6(b).

From the above-mentioned analysis and Fig. 6(a), it can be known that the variation of i_{Lp} exhibits four periods. The current ripples $\triangle i_{Lp1}$, $\triangle i_{Lp2}$, $\triangle i_{Lp3}$, and $\triangle i_{Lp4}$ in these four periods can be expressed as

$$\left|\Delta i_{Lp_1}\right| = \left|\Delta i_{Lp_2}\right| = \left|\Delta i_{Lp_3}\right| = \left|\Delta i_{Lp_4}\right| = \frac{m v_a T_s}{2 V_m L_p}(v_a - v_{Cp}). \tag{5}$$

Thus, in sector 1, the peak-peak current $\triangle i_{Lp,\rm peak}$ of i_{Lp} in one switching period is

$$\Delta i_{Lp_{,\rm peak}} = \frac{m v_a T_s}{2 V_m L_p}(v_a - v_{Cp}). \tag{6}$$

Similarly, there are also four variation periods of inductor current i_{Ln}. The current ripples $\triangle i_{Ln1}$, $\triangle i_{Ln2}$, $\triangle i_{Ln3}$ and $\triangle i_{Ln4}$ in these four periods can be expressed as

$$\begin{cases} \Delta i_{Ln1} = T_s(V_m - m v_a)(v_{Cn} - v_b)/(2L_n V_m) \\ \Delta i_{Ln2} = T_s m(v_{Cn} - v_c)(v_b - v_c)/(2L_n V_m) \\ \Delta i_{Ln3} = T_s\left[V_m - m(v_a - v_c)\right](v_{Cn} - v_b)/(2L_n V_m) \\ \Delta i_{Ln4} = T_s m v_a(v_{Cn} - v_c)/(2L_n V_m) \end{cases}. \tag{7}$$

According to Fig. 6(b), $|\triangle i_{Ln3}|$ and $|\triangle i_{Ln4}|$ are larger than $|\triangle i_{Ln1}|$ and $|\triangle i_{Ln2}|$. Thus, in sector 1, the peak-peak current $\triangle i_{Ln,\rm peak}$ of i_{Ln} in one switching period is

$$\Delta i_{Ln_{,\rm peak}} = \max\left\{\left|\Delta i_{Ln3}\right|, \left|\Delta i_{Ln4}\right|\right\}. \tag{8}$$

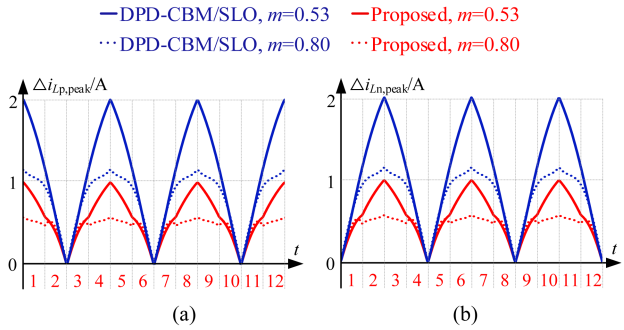

Fig. 7. Peak-peak values of i_{Lp} and i_{Ln} in one input cycle with DPD-CBM, SLO, and the proposed modulation. (a) $\triangle i_{Lp,\text{peak}}$. (b) $\triangle i_{Ln,\text{peak}}$.

TABLE III
CIRCUIT PARAMETERS

Parameters	Value
Inductors L_a, L_b, and L_c	56 μH
Capacitors C_a, C_b, and C_c	880 nF
Capacitors C_p and C_n	880 nF
Inductors L_p and L_n	150 μH
Capacitor C_o	100 μF
Input phase voltage v_{in}	115 V
Output current I_o	5 A
Switching frequency f_s	200 kHz

Similarly, the peak-peak currents $\triangle i_{Lp,\text{peak}}$ and $\triangle i_{Ln,\text{peak}}$ in other sectors can be calculated. Fig. 7 shows the calculation results when $m = 0.80$ and $m = 0.53$, with the circuit parameters are given in Table III.

It can be seen from Fig. 7 that in one input cycle, with the proposed modulation, both $\triangle i_{Lp,\text{peak}}$ and $\triangle i_{Ln,\text{peak}}$ are always smaller than those of DPD-CBM or SLO. The maximum of $\triangle i_{Lp,\text{peak}}$ or $\triangle i_{Ln,\text{peak}}$ is about half that of DPD-CBM or SLO. Both $\triangle i_{Lp,\text{peak}}$ and $\triangle i_{Ln,\text{peak}}$ with DPD-CBM, SLO, and the proposed modulation exhibit fluctuation with the frequency triple that of the input frequency, which is caused by the fluctuation of v_{Cp} and v_{Cn}.

The current ripples with $m = 0.53$ are larger than those with $m = 0.80$, which is caused by the low output voltage v_o. As the absolute averages of v_{Cp} and v_{Cn} are half of v_o, the low v_o will cause the decrease of v_{Cp} and v_{Cn}, which further affects the charging/discharging speed of L_p and L_n, and finally, the larger ripples are obtained.

B. Power Loss Analysis

The total loss consists of switching loss P_{sw}, conduction loss P_{cond}, inductor loss P_{indu} and other power loss, e.g., auxiliary power and snubber loss [14].

1) Switching Loss P_{sw}*:* The switching loss P_{sw} consists of gate driving loss and the power loss during switches turn ON or OFF, and can be calculated as [14]

$$P_{\text{sw}} = V_{ds} I_o t f_s/2 + V_{gs} Q_g f_s \tag{9}$$

where V_{ds} is the drain-source voltage; t is the overlapping period during switches turn ON or OFF; V_{gs} is the gate drive voltage; Q_g is the total gate charge.

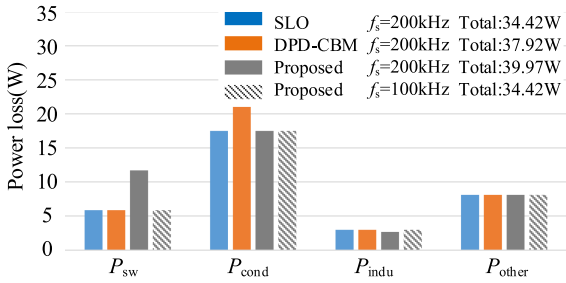

Fig. 8. Total power loss of 3ph-BR with CM filter by using DPD-CBM, SLO and the proposed modulation when $m = 0.80$.

2) Conduction Loss P_{cond}*:* The conduction loss P_{cond} can be calculated as

$$P_{\text{cond}} = I_{Q\_\text{rms}}^2 R_{\text{dson}} + V_F I_{D\_rms} \tag{10}$$

where $I_{Q\cdot\text{rms}}$, R_{dson} are the rms current and on-resistance of switches, respectively; V_F, $I_{D\cdot\text{rms}}$ are the forward voltage and rms current of diodes, respectively.

3) Inductor Loss P_{indu}*:* The inductor loss P_{indu} consists of copper loss and core loss, and can be calculated as

$$P_{\text{indu}} = I_{L\_rms}^2 R_{\text{indu}} + P_V V_e \tag{11}$$

where $I_{L\cdot\text{rms}}$ and R_{indu} are the rms current and resistance of the inductor, respectively; P_v is the core loss per unit volume; V_e is the effective volume of the magnetic core.

According to (9)–(11), when $m = 0.80$, the total loss of 3ph-BR with CM filter by using DPD-CBM, SLO and the proposed modulation can be obtained, as shown in Fig. 8, where the circuit parameters are given in Table III.

It can be seen from Fig. 8, when $f_s = 200$ kHz, the DPD-CBM exhibits the largest conduction loss, which is caused by the elimination of zero vector. In addition, as the proposed modulation completes two charging/discharging cycles of dc-link inductors by increasing the transition number of switches, the higher switching loss is thus obtained, which is approximately twice that of SLO and DPD-CBM. Thus, the proposed modulation with $f_s = 200$ kHz has the highest total loss of 39.97 W.

For a better comparison, the power loss of the proposed modulation with $f_s = 100$ kHz is calculated and provided in Fig. 8. It can be found that the DPD-CBM with $f_s = 200$ kHz exhibits the largest power loss of 37.92 W, while SLO with $f_s = 200$ kHz and the proposed modulation with $f_s = 100$ kHz exhibit the same power loss of 34.42 W.

It can be found from the above analysis that, by increasing the switching frequency from f_s to $2f_s$, DPD-CBM and SLO exhibit the similar switching loss and dc-link current ripples as the proposed modulation. For DPD-CBM, however, its conduction loss is larger than that of the proposed modulation. In addition, due to the employment of the non-nearest vector, its switching harmonic is higher than that of the proposed modulation [8]. For SLO, its vector sequence can cause current distortion [1]. For example, in sector I, the dwell time of vector $\boldsymbol{I}_6$ is smaller than that of $\boldsymbol{I}_1$, and is divided into two parts. Thus, the pulse width is very small and is difficult to realize when v_b is near to zero,

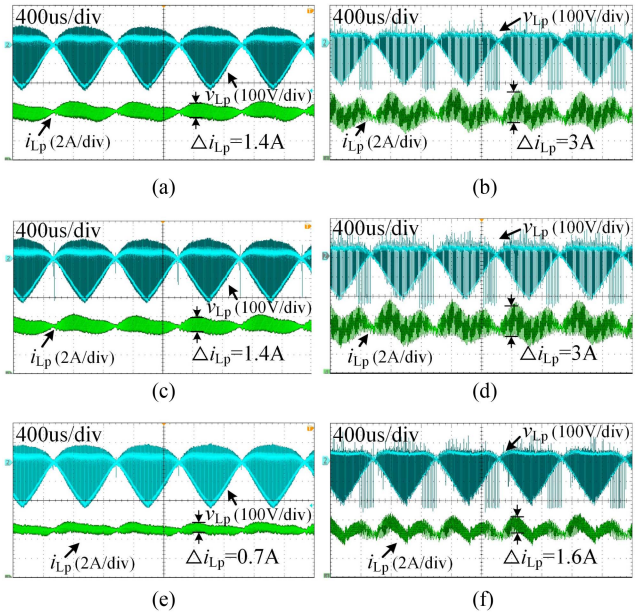

Fig. 9. Experimental results of i_{Lp} and v_{Lp} when $m = 0.80$ with (a) DPD-CBM with $f_s = 200$ kHz. (b) DPD-CBM with $f_s = 100$ kHz. (c) SLO with $f_s = 200$ kHz. (d) SLO with $f_s = 100$ kHz. (e) Proposed modulation with $f_s = 200$ kHz. (f) Proposed modulation with $f_s = 100$ kHz.

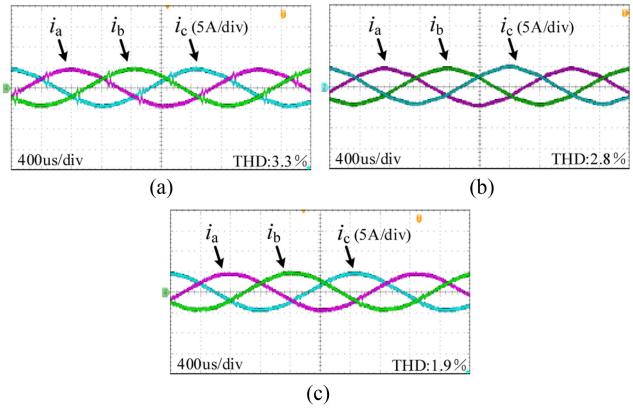

Fig. 10. Experimental results of input currents when $m = 0.80, f_s = 200$ kHz with different modulation. (a) DPD-CBM. (b) SLO. (c) Proposed modulation.

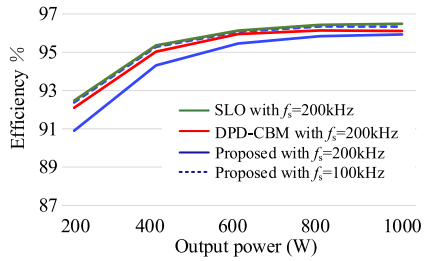

Fig. 11. Efficiency curve of 3ph-BR with CM filter when $m = 0.80$ by using DPD-CBM, SLO, and the proposed modulation.

which will cause current distortion and increase the THD of input currents, as discussed in [1]. Especially with the increase of f_s, the resolution of pulse width generated by the controller usually decreases, which further deteriorates the input current quality. Therefore, increasing the switching frequency of DPD-CBM or SLO to optimize the dc-link current ripple is not suitable.

IV. Experimental Results

To verify the effectiveness of the proposed modulation, a 1-kW prototype is built, with the circuit parameters as given in Table III. In the experimental prototype, microprocessor DSPIC33EP64GS505 and MOSFETs STD18N65 are used.

A. Experimental Results of 3ph-BR With CM Filter When m = 0.80

Fig. 9 shows the experimental results of i_{Lp} and v_{Lp} with DPD-CBM, SLO, and the proposed modulation, respectively, when switching frequency $f_s = 200$ kHz or $f_s = 100$ kHz. As the waveforms of i_{Lp} and i_{Ln} only exhibit the phase difference, the waveform of i_{Ln} is not provided. Due to the parasitic inductance of the measuring equipment, v_{Lp} exhibits some spikes, which can be improved by using the equipment with small parasitic inductance.

It can be seen that both DPD-CBM and SLO exhibit the similar current ripples with $\triangle i_{Lp} = 1.4$ A when $f_s = 200$ kHz and $\triangle i_{Lp} = 3$ A when $f_s = 100$ kHz. By using the proposed modulation, $\triangle i_{Lp} = 0.7$A when $f_s = 200$ kHz and $\triangle i_{Lp} = 1.6$ A when $f_s = 100$ kHz, which are about half those of DPD-CBM and SLO. Thus, the proposed modulation suppresses the dc-link current ripple.

Fig. 10 shows the experimental results of the input currents with DPD-CBM, SLO, and the proposed modulation, respectively. The THDs of the input currents of DPD-CBM, SLO, and the proposed modulation are 3.3%, 2.8%, and 1.9%, respectively. The DPD-CBM and SLO exhibit higher THD, which is consistent with the analysis in Section III-B.

Fig. 11 shows the efficiency curve of 3ph-BR with CM filter by using DPD-CBM, SLO, and the proposed modulation. It can be seen that the efficiency of the proposed modulation with $f_s = 200$ kHz is about 96% under the output power of 1000 W, which is slightly lower than that of DPD-CBM by 0.2% and SLO by 0.5%. As the purpose of the proposed modulation is to suppress the dc-link current ripple of the 3ph-BR with CM filter, such a slight decrease of efficiency is acceptable.

By using the proposed modulation with $f_s = 100$ kHz, the similar efficiency to SLO is obtained, and is higher than that of DPD-CBM. When the output power is 1000 W, the total losses of DPD-CBM, SLO, proposed modulation with $f_s = 200$ kHz or $f_s = 100$ kHz are 38.9, 35.1, 40.7, and 36.1 W, respectively, which are close to the theoretical calculation in Section III-B.

B. Experimental Results of 3ph-BR With CM Filter When m = 0.53

When $m = 0.53$ and $f_s = 200$ kHz, Fig. 12 shows the experimental results of i_{Lp} and v_{Lp} with DPD-CBM, SLO, and the proposed modulation, respectively. Similarly, i_{Lp} with the proposed modulation also exhibits a smaller ripple than

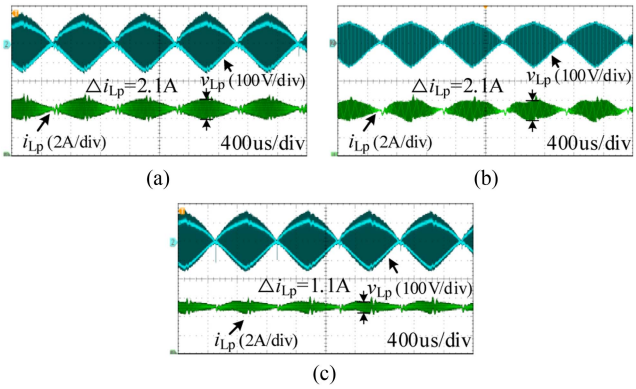

Fig. 12. Experimental results of i_{Lp} and v_{Lp} when $m = 0.53$, $f_s = 200$ kHz with different modulations. (a) DPD-CBM. (b) SLO. (c) Proposed modulation.

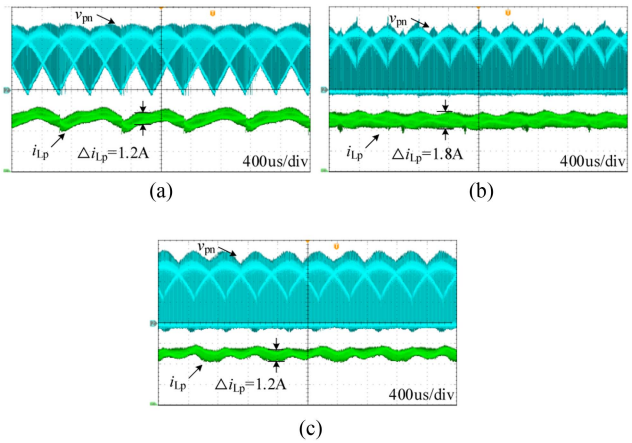

Fig. 13. Experimental results of i_{Lp} and v_{Lp} for 3ph-BR without CM filter when $m = 0.80$, $f_s = 200$ kHz with different modulation. (a) DPD-CBM. (b) SLO. (c) Proposed modulation.

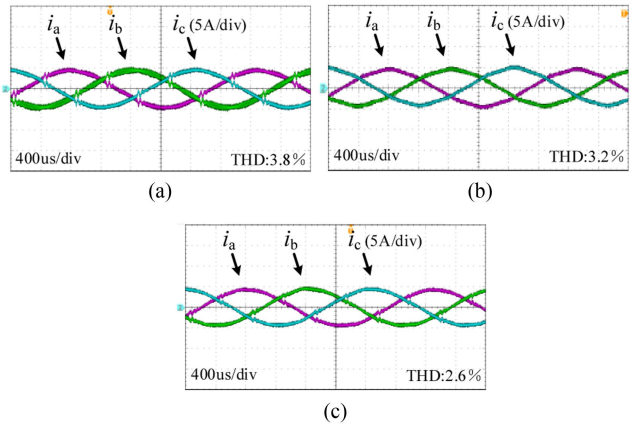

Fig. 14. Experimental results of input currents for 3ph-BR without CM filter when $m = 0.80$, $f_s = 200$ kHz with different modulation. (a) DPD-CBM. (b) SLO. (c) Proposed modulation.

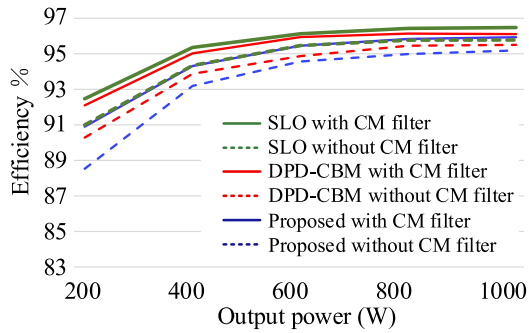

Fig. 15. Efficiency curve of 3ph-BR with or without CM filter when $m = 0.80$, $f_s = 200$ kHz by using DPD-CBM, SLO, and the proposed modulation.

DPD-CBM and SLO. In addition, both the current ripples under DPD-CBM, SLO, and the proposed modulation are larger than those when $m = 0.80$, which is caused by the low output voltage v_o, as discussed in Section III-A.

C. Experimental Results of 3ph-BR Without CM Filter

When $m = 0.80$ and $f_s = 200$ kHz, Fig. 13 shows the experimental result of i_{Lp} for 3ph-BR without CM filter by using DPD-CBM, SLO, and the proposed modulation. It can be seen that $\triangle i_{Lp} = 1.8$ A with SLO while $\triangle i_{Lp} = 1.2$ A with DPD-CBM and the proposed modulation. Thus, the proposed modulation can also be used to optimize the dc-link current ripple of 3ph-BR without CM filter.

Fig. 14 shows the experimental result of input currents for 3ph-BR without CM filter when $m = 0.80$ and $f_s = 200$ kHz, with DPD-CBM, SLO, and the proposed modulation, respectively. The THDs of the input currents are 3.8%, 3.2%, and 2.6%, respectively.

It is worth noting that the THD of the 3ph-BR without a CM filter is higher than that of 3ph-BR with CM filter. Compared with the 3ph-BR with a CM filter, more CM noise conducts through the system for the 3ph-BR without CM filter, which flows through the input port and deteriorates the input currents [10]. Thus, a higher THD of input currents is produced.

Fig. 15 shows the efficiency of 3ph-BR with or without CM-filter, by using DPD-CBM, SLO, and the proposed modulation, respectively. It can be seen that the 3ph-BR with the CM filter has higher efficiency than the 3ph-BR without the CM filter. The CM noise can cause larger block voltage on switching devices, which will increase the switching loss [12]. Thus, the 3ph-BR without a CM filter exhibits the lower efficiency.

V. Conclusion

An optimized modulation of the 3ph-BR with the CM filter for dc-link current ripple suppression is proposed in this letter. By optimizing the vector pattern, both dc-link inductors L_p and L_n complete two charging/discharging cycles within one switching period. Thus, the dc-link current ripples can be suppressed. Both the theoretical analysis and experimental results show that $\triangle i_{Lp,\text{peak}}$ and $\triangle i_{Ln,\text{peak}}$ of the proposed method are only about half those of the conventional modulation. Thus, the proposed modulation is an attractive solution for the 3ph-BR with the CM filter to suppress the dc-link current ripples.

REFERENCES

[1] R. Huang, J. Xu, Q. Chen, X. Guo, and C. Zhou, "An optimized asymmetric modulation scheme for three-phase buck rectifier without input current distortion at the sector boundaries," *IEEE Trans. Power Electron.*, vol. 37, no. 12, pp. 14040–14044, Dec. 2022.

[2] Q. Chen, J. Xu, Z. Tao, H. Ma, and C. Chen, "Analysis of sector update delay and its effect on digital control three-phase six-switch buck PFC converters with wide AC input frequency," *IEEE Trans. Power Electron.*, vol. 36, no. 1, pp. 931–946, Jan. 2021.

[3] C. Saber, D. Labrousse, B. Revol, and A. Gascher, "Challenges facing PFC of a single-phase on-board charger for electric vehicles based on a current source active rectifier input stage," *IEEE Trans. Power Electron.*, vol. 31, no. 9, pp. 6192–6202, Sep. 2016.

[4] S. Gangavarapu and A. K. Rathore, "Three phase buck–boost derived PFC converter for more electric aircraft," *IEEE Trans. Power Electron.*, vol. 34, no. 7, pp. 6264–6275, Jul. 2019.

[5] R. M. Cuzner and G. Venkataramanan, "Current source rectifiers in discontinuous conduction modes of operation," *IEEE Trans. Ind. Appl.*, vol. 51, no. 1, pp. 470–478, Jan./Feb. 2015.

[6] T. Halkosaari and H. Tuusa, "Optimal vector modulation of a PWM current source converter according to minimal switching losses," in *Proc. IEEE 31st Annu. Power Electron. Specialists Conf.*, 2000, vol. 1, pp. 127–132.

[7] X. Guo, Y. Yang, and X. Wang, "Optimal space vector modulation of current-source converter for DC-link current ripple reduction," *IEEE Trans. Ind. Electron.*, vol. 66, no. 3, pp. 1671–1680, Mar. 2019.

[8] L. Ming, W. Ding, P. C. Loh, and Z. Xin, "A direct carrier-based modulation scheme with full index range for DC-link current ripple mitigation of a current source converter," *IEEE Trans. Ind. Electron.*, vol. 69, no. 1, pp. 452–462, Jan. 2022.

[9] X. Guo and L. Xun, "A new current ripple suppression strategy for DC link inductance of three-phase current source converter," *IEEE Trans. Ind. Electron.*, vol. 70, no. 10, pp. 9700–9708, Oct. 2023.

[10] Q. Chen, J. Xu, L. Wang, R. Huang, and H. Ma, "Analysis and improvement of the effect of distributed parasitic capacitance on high-frequency high-density three-phase buck rectifier," *IEEE Trans. Power Electron.*, vol. 36, no. 6, pp. 6415–6428, Jun. 2021.

[11] R. Huang, J. Xu, Q. Chen, X. Guo, and H. Cao, "Reconstructed phase voltages based power following control for three-phase buck rectifier under unbalanced phase voltages and wide AC input frequency," *IEEE Trans. Power Electron.*, vol. 38, no. 2, pp. 2022–2031, Feb. 2023.

[12] H. Cao, P. Yang, X. Guo, R. Huang, and J. Xu, "An improved asymmetric modulation of current-source rectifier with CM filter for low voltage stress on switching devices," *IEEE Trans. Power Electron.*, vol. 38, no. 7, pp. 7964–7970, Jul. 2023.

[13] B. N. Sanusi, M. Zambach, C. Frandsen, M. Beleggia, A. Michael Jørgensen, and Z. Ouyang, "Investigation and modeling of DC bias impact on core losses at high frequency," *IEEE Trans. Power Electron.*, vol. 38, no. 6, pp. 7444–7458, Jun. 2023.

[14] A. K. Singh, E. Jeyasankar, P. Das, and S. K. Panda, "A matrix-based non-isolated three-phase AC–DC rectifier with large step-down voltage gain," *IEEE Trans. Power Electron.*, vol. 32, no. 6, pp. 4796–4811, Jun. 2017.